Inorg. Chem. **2009**, *48*, 3095−3103

Symmetric Heteropolynuclear Ti(IV)/Cu(I) Complexes Exhibiting Stepwise Electrochemical Reductions to Ti(III) Species

Pierre Le Gendre,*,† Virginie Comte,† Marie-Joëlle Ondel-Eymin,† Claude Moïse,† Eveline Pousson,† Philippe Richard,† Yves Mugnier,*,† Daniel Fortin,‡ René T. Boeré,§ and Pierre D. Harvey‡

Institut de Chimie Moléculaire de l'Université de Bourgogne (ICMUB) UMR CNRS 5260, Faculté des Sciences Mirande, Université de Bourgogne, 9 avenue Alain Savary, BP 47870, 21078 Dijon Cedex, France, Department of Chemistry and Biochemistry, University of Lethbridge, Lethbridge, T1K 3M4 Alberta, Canada, and Département de Chimie, Université de Sherbrooke, Sherbrooke, J1K 2R1 Québec, Canada

Received December 15, 2008

The heterotrinuclear complexes, $[(CpTiCl_2Cp\text{-}PPh_2)_2Cu]^+$ (**2**) (as PF_6^- salt) and $[CpTiCl_2Cp\text{-}PPh_2]_2CuCl$ (**3**), containing two electron-poor Ti(IV) fragments and one electron-rich Cu(I) center, and a tetrametallic species, $[(CpTiCl_2Cp\text{-}PPh_2)Cu(\mu\text{-}Cl)]_2$ (**4**), were synthesized and characterized. The trinuclear nature of **2** and **3** was demonstrated by X-ray crystallography for which the three metallic centers are held together by two $CpPPh_2$ ligands. Weak Cl···Cu interactions are noted in **3**, whereas two stronger Cl−Cu bridges are depicted in the cationic complex **2**. The tetranuclear complex **4** contains two Cu atoms bridged together by two chloride ligands and connected to one Ti atom by one $CpPPh_2$ ligand and one μ-Cl ligand. Despite the short distances in the Ti−Cl−Cu bridges, notably in **2** and **4**, the NMR spectra reveals evidence of fluxion in solution attributed to the lability of the μ-Cl ligands. Electrochemical experiments performed on **2** (rotating disk electrode and cyclic voltammograms) demonstrated the presences of two successive 1-electron reductions generating a first structurally unsymmetrical paramagnetic species $[(CpTiCl_2Cp\text{-}PPh_2)_2Cu]^0$ (**2′**), confidently characterized by electron paramagnetic resonance (EPR) as a Ti(III)−Cu(I)−Ti(IV) system, and a second one, which is tentatively assigned to a symmetric neutral complex formulated as $[CpTiClCp\text{-}PPh_2]_2CuCl$ (**5**) with an EPR signature indistinguishable from that of **2′** (i.e., Ti(III)−Cu(I)−Ti(III) system with a similar electronic environment). Density functional theory (DFT) computations examining the nature of the frontier orbitals and the geometry confirmed the presence and lack of symmetry in **2** and **2′**, respectively. The detection of chemical/electrochemical mechanisms in the electrochemical studies provides a clear explanation for the stepwise reduction behavior in these systems through chloride ligand transfer from Ti to Cu prior to the first reduction step. This transfer process is fully reversible upon re-oxidation. The electrochemical properties of complexes **3** and **4** are also reported.

Introduction

"Early-late" heterobimetallic complexes represent a promising list of catalysts owing to the potential cooperative reactivity of very different metals.[1,2] However, on the basis of the literature, most of the synergisms reported to date have been attributed to very subtle interactions between both metallic centers which would have been difficult to foresee.[3] Therefore the design of heterobimetallic catalysts for a target reaction is a very difficult task. The quest requires finding compatible organometallic fragments and anticipating the nature and magnitude of the neighboring metal−metal interactions while the coordination spheres and electronic characteristics of both metallic centers will probably change several times throughout the catalytic process. Our strategy to study such systems was to first synthesize a large library of early metal ligands and then to react these metalloligands with late transition metals. Thus, we obtained a series of

* To whom correspondence should be addressed. E-mail: pierre.le-gendre@u-bourgogne.fr (P.L.-G.), boere@uleth.ca (Y.M.).
† Université de Bourgogne.
‡ Université de Sherbrooke.
§ University of Lethbridge.

(1) (a) Gade, L. H. *Angew. Chem., Int. Ed.* **2000**, *39*, 2659. (b) Wheatley, N.; Kalck, P. *Chem. Rev.* **1999**, 3379. (c) Stephan, D. W. *Coord. Chem. Rev.* **1989**, *95*, 41.

10.1021/ic8023869 CCC: $40.75
Published on Web 03/02/2009

early late heterobimetallic complexes (Ti/Ru, Ta/Ru, Ti/Rh) in sufficient amounts to carry out a screening of their catalytic properties.[4] Useful insights on the influence of the early metal fragment on its late metal neighbor were readily obtained by comparing the catalytic properties of the bimetallic complexes with their corresponding monometallic analogues. Concomitantly, electrochemical methods were shown to be particularly useful in the understanding of the subtle metal−metal interactions observed in these systems.[5] In attempts to explore similar interactions, we recently prepared a series of polynuclear complexes binding titanocene fragments to coinage metals (Ag, Au, Cu). We now wish to report the synthesis and structural analysis of three novel heteropolymetallic (Ti/Cu) complexes. The electrochemical properties of these complexes were also investigated, and the characterization by electron paramagnetic resonance (EPR) spectroscopy of the reduced species is reported as well. Evidence for compatibility of both metals in different oxidation states is observed.

Experimental Section

All reactions were carried out under an atmosphere of purified argon using vacuum line techniques. Solvents were dried and distilled under argon from sodium before use.

Apparatus. Elemental analyses were performed with an EA 1108 CHNS-O FISONS Instrument. ^{1}H- (500 MHz), ^{13}C- (125.8 MHz), and ^{31}P- (202.5 MHz) NMR spectra were recorded with a Bruker 500 Avance spectrometer. Chemical shifts are quoted in ppm (δ) relative to TMS (^{1}H, ^{13}C) or external H_3PO_4 (^{31}P). Coupling constants are reported in hertz. The titanocene phosphane **1** was synthesized as reported previously.[6]

Synthesis of $[(CpTiCl_2Cp\text{-}PPh_2)_2Cu]^+$; PF_6^- (2). A 10 mL Schlenk flask was charged under argon with **1** (100 mg, 0.23 mmol) and $Cu(MeCN)_4PF_6$ (43 mg, 0.115 mmol). 8 mL of degassed benzene were added, and the mixture was stirred at room temperature for 4 h during which a pink precipitate slowly formed. The solvent was removed by filtration, and the red residue was dried under vacuum. The crude product was recrystallized from dichloromethane-hexane to afford red crystals (68 mg, 55% yield). Anal. Calcd for $C_{44}H_{38}P_3Cl_4Ti_2CuF_6$ (1074.78): C, 49.17; H, 3.56. Found: C, 49.83; H, 4.02. ^{31}P{^{1}H} NMR (CD_2Cl_2): $\delta = -3.1$ (broad signal), -144.4 (hept, $^1J_{PF} = 708$ Hz, PF_6). ^{1}H NMR (CD_2Cl_2): $\delta =$ 7.55−7.23 (m, 20H, Ph), 6.73 (m, 4H, C_5H_4), 6.53 (s, 10H, C_5H_5), 6.44 (m, 4H, C_5H_4). ^{13}C{^{1}H} NMR (CD_2Cl_2): $\delta = 134.4$ (8C, Ph), 133.6 (4C, Ph, broad signal), 131.2 (4C, Ph, broad signal), 129.0 (8C, Ph), 128.2 (2C, C_5H_4), 122.0 (4C, C_5H_4), 121.6 (10C, C_5H_5), 120.8 (4C, C_5H_4).

Synthesis of $[CpTiCl_2Cp\text{-}PPh_2]_2CuCl$ (3). This compound was obtained as a red powder following the same procedure as for **2** except that 0.5 molar equiv of CuCl (11.4 mg, 0.115 mmol) was used. The crude product was recrystallized from dichloromethane-hexane to give red crystals (92 mg, 83% yield). Anal. Calcd for $C_{44}H_{38}P_2Cl_5Ti_2Cu$ (965.27): C, 54.75; H, 3.97. Found: C, 54.95; H, 4.00. ^{31}P{^{1}H} NMR ($CDCl_3$): $\delta = -11.9$ ppm (broad signal). ^{1}H NMR ($CDCl_3$): $\delta =$ 7.35−7.17 (m, 20H, Ph), 6.92 (m, 4H, C_5H_4), 6.57 (s, 10H, C_5H_5), 6.51 (m, 4H, C_5H_4). ^{13}C{^{1}H} NMR ($CDCl_3$): $\delta = 134.1$ (8C, Ph), 132.3 (d, $^1J_{CP} = 30$ Hz, 4C, Ph), 130.3 (4C, Ph), 128.7 (8C, Ph), 127.6 (2C, C_5H_4), 126.0 (4C, C_5H_4), 121.9 (10C, C_5H_5), 121.2 (4C, C_5H_4).

Synthesis of $[(CpTiCl_2Cp\text{-}PPh_2)Cu(\mu\text{-}Cl)]_2$ (4). This compound was prepared according to the same procedure as for **2** except that 1 molar equiv of CuCl (22.8 mg, 0.23 mmol) was used. It was obtained as a pink powder. This crude product was recrystallized from dichloromethane-hexane to give red crystals (86 mg, 70% yield). Anal. Calcd for $C_{44}H_{38}P_2Cl_6Ti_2Cu_2$ (1064.26): C, 49.66; H, 3.60. Found: C, 48.94; H, 3.61. ^{31}P{^{1}H} NMR ($CDCl_3$): $\delta = -5.9$ ppm (broad signal). ^{1}H NMR ($CDCl_3$): $\delta =$ 7.61−7.29 (m, 20H, Ph), 6.63 (m, 4H, C_5H_4), 6.59 (m, 4H, C_5H_4), 6.54 (s, 10H, C_5H_5). ^{13}C{^{1}H} NMR ($CDCl_3$): $\delta = 134.5$ (8C, Ph), 131.5 (4C, Ph), 130.9 (4C, Ph), 129.0 (8C, Ph), 127.0 (2C, C_5H_4), 126.1 (4C, C_5H_4), 121.6 (10C, C_5H_5), 119.3 (4C, C_5H_4).

Electrochemical Experiments. All manipulations were performed using Schlenk techniques in an atmosphere of dry oxygen-free argon. The supporting electrolyte $[N(nBu)_4][PF_6]$ was degassed under vacuum before use and then dissolved to a concentration of 0.2 mol L^{-1}. For cyclic voltammetry experiments, the concentration of the analyte was almost 10^{-3} mol·L^{-1}. Voltammetric analyses were carried out in a standard three electrode cell using an EG&G Princeton Applied Research (PAR) Model 263A potentiostat, interfaced to a computer running Electrochemistry Power Suite software. The reference electrode was an Ag/Ag^+ separated from the solution by a sintered glass disk. The auxiliary electrode was a platinum wire. For all voltammetric measurements, the working electrode was a vitreous carbon disk ($\Phi = 3$ mm). The controlled potential electrolysis was performed with an Amel 552 potentiostat coupled with an Amel 721 electronic integrator. Bulk electrolyses were performed in a cell with three compartments separated with

(2) (a) Moriya, M.; Fröhlich, R.; Kehr, G.; Erker, G.; Grimme, S. *Chem.—Asian. J.* **2008**, *3*, 753. (b) Hernandez-Gruel, M. A. F.; Lahoz, F. J.; Dobrinovich, I. T.; Javier Modrego, F.; Oro, L. A.; Pérez-Torrente, J. J. *Organometallics* **2007**, *26*, 2616. (c) Fandos, R.; Gallego, B.; Otero, A.; Rodriguez, A.; Ruiz, M. J.; Terrerosd, P.; Pastore, C. *J. Chem. Soc., Dalton Trans.* **2006**, 2683. (d) Cornelissen, C.; Erker, G.; Kehr, G.; Fröhlich, R. *Organometallics* **2005**, *24*, 214. (e) Griffith, C. S.; Koutsantonis, G. A.; Skelton, B. W.; White, A. H. *Angew. Chem., Int. Ed.* **2005**, *44*, 3038. (f) Stempfle, B.; Gevert, O.; Werner, H. *J. Organomet. Chem.* **2003**, *681*, 70. (g) Braunstein, P.; Morise, X.; Bénard, M.; Rohmer, M.-M.; Welter, R. *Chem. Commun.* **2003**, 610. (h) Wenzel, B. W.; Lönnecke, P.; Hey-Hawkins, E. *Organometallics* **2002**, *21*, 2070. (i) Hofmann, M.; Malisch, W.; Schumacher, D.; Lager, M.; Nieger, M. *Organometallics* **2002**, *21*, 3485. (j) Kuwata, S.; Kabashima, S.-I.; Sugiyama, N.; Ishii, Y.; Hidai, M. *Inorg. Chem.* **2001**, *40*, 2034. (k) Mattheis, C.; Braunstein, P.; Fischer, A. *J. Chem. Soc., Dalton Trans.* **2001**, 800. (l) Nagano, T.; Kuwata, S.; Ishii, Y.; Hidai, M. *Organometallics* **2000**, *19*, 4176. (m) Graham, T. W.; Llamazares, A.; McDonald, R.; Cowie, M. *Organometallics* **1999**, *18*, 3502.

(3) (a) Kuwabara, J.; Takeuchi, D.; Osakada, K. *Chem. Commun.* **2006**, 3815. (b) Morgan, J. P.; Kundu, K.; Doyle, M. P. *Chem. Commun.* **2005**, 3307. (c) Hernandez-Gruel, M. A. F.; Pérez-Torrente, J. J.; Ciriano, M. A.; Rivas, A. B.; Lahoz, F. J.; Dobrinovitch, I. T.; Oro, L. A. *Organometallics* **2003**, *22*, 1237. (d) Bosch, B. E.; Brümmer, I.; Kunz, K.; Erker, G.; Fröhlich, R.; Kotila, S. *Organometallics* **2000**, *19*, 1255. (e) Casado, M. A.; Pérez-Torrente, J. J.; Ciriano, M. A.; Oro, L. A.; Orejón, A.; Claver, C. *Organometallics* **1999**, *18*, 3035. (f) Yamaguchi, Y.; Susuki, N.; Mise, T.; Wakatsuki, Y. *Organometallics* **1999**, *18*, 996. (g) Green, M. L. H.; Popham, N. H. *J. Chem. Soc., Dalton Trans.* **1999**, 1049. (h) Senocq, F.; Randrianalimanana, C.; Thorez, A.; Kalck, P.; Choukroun, R.; Gervais, D. *Chem. Commun.* **1984**, 1376.

(4) (a) Borguet, Y.; Delfosse, S.; Sauvage, X.; Delaude, L.; Demonceau, A.; Bareille, L.; Le Gendre, P.; Moïse, C. *Polym. Prepr.* **2008**, *49*, 24. (b) Goux, J.; Le Gendre, P.; Richard, P.; Moïse, C. *J. Organomet. Chem.* **2005**, *690*, 301. (c) Comte, V.; Le Gendre, P.; Richard, P.; Moïse, C. *Organometallics* **2005**, *24*, 1439. (d) Le Gendre, P.; Comte, V.; Michelot, A.; Moïse, C. *Inorg. Chim. Acta* **2003**, *350*, 289. (e) Le Gendre, P.; Picquet, M.; Richard, P.; Moïse, C. *; J. Organomet. Chem.* **2002**, *231*, 643.

(5) Cattey, H.; Vallat, A.; Le Gendre, P.; Evrard, D.; Moïse, C.; Mugnier, Y. *New J. Chem.* **2005**, *29*, 1302.

(6) (a) Le Gendre, P.; Richard, P.; Moïse, C. *J. Organomet. Chem.* **2000**, *605*, 151. (b) Leblanc, J. C.; Moïse, C.; Maisonnat, A.; Poilblanc, R.; Charrier, C.; Mathey, F. *J. Organomet. Chem.* **1982**, *231*, C43.

Table 1. Crystal and Structure Refinement Data for **2**, **3**, and **4**

compounds	**2**	**3**	**4**
empirical formula	$C_{45}H_{40}Cl_6Cu\ F_6P_3Ti_2$	$C_{47}H_{44}Cl_{11}CuP_2Ti_2$	$C_{46}H_{42}Cl_{10}Cu_2P_2Ti_2$
formula weight	1159.72	1220.05	1234.08
temperature (K)	115(2)	115(2)	115(2)
crystal system	monoclinic	triclinic	monoclinic
space group	$P2_1/n$	$P\bar{1}$	$P2_1/c$
a (Å)	18.8888(6)	10.5750(1)	9.5770(2)
b (Å)	12.0637(4)	15.2335(2)	15.5025(3)
c (Å)	22.7268(8)	17.1021(3)	17.1445(3)
α (deg)		76.149(1)	
β (deg)	91.628(1)	80.156(1)	93.380(1)
γ (deg)		69.941(1)	
volume (Å^3)	5176.6(3)	2500.72(6)	2540.97(8)
Z	4	2	2
$\rho_{calc.}$ (g/cm^3)	1.488	1.620	1.613
μ (mm^{-1})	1.163	1.419	1.750
size (mm^3)	0.17 × 0.10 × 0.05	0.25 × 0.25 × 0.08	0.37 × 0.37 × 0.07
F(000)	2336	1232	1240
λ	0.71073	0.71073	0.71073
θ range (deg)	1.91−27.47	2.06−27.52	2.88−27.52
index ranges	h: −24; 24	h: −13; 13	h: −12; 12
	k: −13; 15	k: −19; 19	k: −20; 19
	l: −29; 29	l: −22; 22	l: −22; 22
reflections collected	21252	20106	18486
R_{int}	0.033	0.028	0.043
reflections with $I \geq 2\sigma(I)$	9871	8792	5804
data/restraints/param.	11701/0/549	11430/0/568	5804/0/280
final R indices [$I \geq 2\sigma(I)$]	$R1^a = 0.0551$	$R1^a = 0.0340$	$R1^a = 0.0358$
	$wR2^b = 0.1274$	$wR2^b = 0.0701$	$wR2^b = 0.0847$
R indices (all data)	$R1^a = 0.0675$	$R1^a = 0.0541$	$R1^a = 0.0471$
	$wR2^b = 0.1359$	$wR2^b = 0.0758$	$wR2^b = 0.0903$
goodness-of-fit^c on F^2	1.098	1.049	1.041
$\Delta\rho$ (e Å^{-3})	1.735 and −1.410	1.000 and −0.752	0.880 and −0.917
CCDC deposition no.			

^{a} $R1 = \sum||F_o| - |F_c||/\sum|F_o|$. ^{b} $wR2 = \{\sum[w(F_o^2 - F_c^2)^2]/\sum w(F_o^2)^2\}^{1/2}$ where $w = 1/[\sigma^2(F_o^2 + (0.0425P)^2 + 17.31P]$ for **2**, $w = 1/[\sigma^2(F_o^2 + (0.0280P)^2 + 0.52P]$ for **3**, and $w = 1/[\sigma^2(F_o^2 + (0.0432P)^2 + 2.44P]$ for **4** where $P = (\max(F_o^2,0)+2F_c^2)/3$. ^{c} $S = [\sum w(F_o^2 - F_c^2)^2/(n - p)]^{1/2}$ (n = number of reflections, p = number of parameters).

glass frits of medium porosity. Carbon gauze was used as the working electrode, a platinum plate as the counter-electrode, and a saturated calomel electrode as the reference electrode.

X-ray Structure Determination of Compounds 2, 3, and 4. Intensity data were collected at 115 K on a Nonius Kappa CCD for **3** and **4**, while an APEX II detector was used for **2**. The structures were solved by direct methods (SIR92)[7] and refined with full-matrix least-squares methods based on F^2 (SHELXL-97)[8] with the aid of the WINGX program.[9] All non-hydrogen atoms were refined with anisotropic thermal parameters. Hydrogen atoms were included in their calculated positions and refined with a riding model. For **2**, the difference Fourier map clearly indicates the presence of a disordered dichloromethane solvent molecule which was included in the model with a converged occupancy factor of 0.32. Unfortunately, although a large void of about 578 Å^3 was estimated by the aid of the PLATON program,[10] the residual electron density is too unclear and diffuse to successfully locate and model other parts of the disordered solvent molecule(s). Crystallographic data are reported in Table 1.

Computations. The complexes were optimized with the ONIOM layers option included in Gaussian 03.[11] The high level frame containing the Cu, Ti, Cl, P, and the cyclopentadienyl carbons were treated by DFT B3LYP and 3-21G* basis sets and core potentials. The low level containing the residual carbons and hydrogen was treated with molecular mechanics UFF and STO-3G basis sets. The final EPR and energy calculations were obtained by DFT B3LYP including all the atoms, with 6-31G basis sets on the C, H, and 3-21G* basis sets on the Cu, Ti, Cl, and P atoms.

Results and Discussion

The choice of the bridging ligand plays a major role in the binding of metal atoms with very different electronic configurations such as Ti(IV) (d^{10}) and a Cu(I) (d^{10}). Stephan and co-workers have shown that thiolates are suitable ligands in that respect.[12] This group also reported the synthesis of the titanium complex $Cp_2Ti(SCH_2CH_2PPh_2)_2$ which is capable of acting as a bidentate metalloligand for Cu(I).[13]

(7) Altomare, A.; Cascarano, G.; Giacovazzo, C.; Guagliardi, A. *J. Appl. Crystallogr.* **1993**, *26*, 343.
(8) Sheldrick, G. M., Institüt für Anorganische Chemie der Universität, Tammanstrasse 4, D-3400 Göttingen, Germany, 1998.
(9) Farrugia, L. J. *J. Appl. Crystallogr.* **1999**, *32*, 837.
(10) Spek, A. L. *J. Appl. Crystallogr.* **2003**, *36*, 7.
(11) Frisch, M. J.; Trucks, G. W.; Schlegel, H. B.; Scuseria, G. E.; Robb, M. A. Cheeseman, J. R.; Montgomery, Jr., J. A.; Vreven, T.; Kudin, K. N.; Burant, J. C.; Millam, J. M.; Iyengar, S. S.; Tomasi, J.; Barone, V.; Mennucci, B.; Cossi, M.; Scalmani, G.; Rega, N.; Petersson, G. A.; Nakatsuji, H.; Hada, M.; Ehara, M.; Toyota, K.; Fukuda, R.; Hasegawa, J.; Ishida, M.; Nakajima, T.; Honda, Y.; Kitao, O.; Nakai, H. ; Klene, M.; Li, X.; Knox, J. E.; Hratchian, H. P.; Cross, J. B.; Adamo, C.; Jaramillo, J.; Gomperts, R.; Stratmann, R. E.; Yazyev, O.; Austin, A. J.; Cammi, R.; Pomelli, C.; Ochterski, J. W.; Ayala, P. Y.; Morokuma, K.; Voth, G. A.; Salvador, P.; Dannenberg, J. J.; Zakrzewski, V. G.; Dapprich, S.; Daniels, A. D.; Strain, M. C.; Farkas, O.; Malick, D. K.; Rabuck, A. D.; Raghavachari, K.; Foresman, J. B; . Ortiz, J. V.; Cui, Q.; Baboul, A. G.; Clifford, S.; Cioslowski, J.; Stefanov, B. B.; Liu, G.; Liashenko, A.; Piskorz, P.; Komaromi, I.; Martin, R. L.; Fox, D. J.; Keith, T.; Al-Laham, M. A.; Peng, C. Y.; Nanayakkara, A.; Challacombe, M.; Gill, P. M. W.; Johnson, B.; Chen, W.; Wong, M. W.; Gonzalez, C.; Pople, J. A. *Gaussian 03*, Revision C.02; Gaussian, Inc.: Wallingford, CT, 2004.
(12) Wark, T. A.; Stephan, D. W. *Inorg. Chem.* **1987**, *26*, 363.

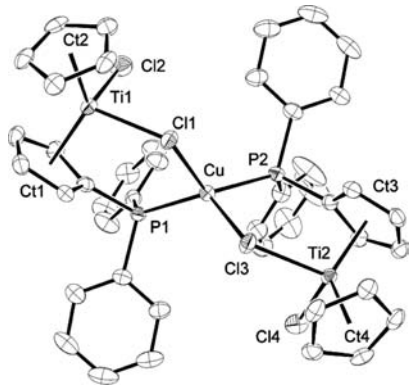

Figure 1. ORTEP representation of $[(CpTiCl_2Cp\text{-}PPh_2)_2Cu]^+$ (**2**) as PF_6^- salt. The thermal ellipsoids are shown at 50% probability. The H-atoms, the solvent, and the PF_6^- anion are not shown for clarity. Selected bond distances (Å) and angles (deg): Cu−P(1), 2.2369(9), Cu−P(2), 2.2312(9); Cu−Cl(1), 2.4110(9); Cu−Cl(3), 2.4327(9); Ti(1)−CT(1), 2.0807(8); Ti(1)−CT(2), 2.0559(9); Ti(1)−Cl(1), 2.3894(9); Ti(1)−Cl(2), 2.3283(11); Ti(2)−CT(3), 2.0825(8); Ti(2)−CT(4), 2.0551(8); Ti(2)−Cl(3), 2.3891(9); Ti(2)−Cl(4), 2.3365(11); Ti(1)−Cl(1)−Cu, 116.12(4); Ti(2)−Cl(3)−Cu, 117.85(4); CT(1)−Ti(1)−CT(2), 131.17(7); Cl(2)−Ti(1)−Cl(1), 94.64(4); CT(3)−Ti(2)−CT(4), 130.97(7); Cl(3)−Ti(2)−Cl(4), 93.73(4); P(1)−Cu−P(2), 128.81(4); P(2)−Cu−Cl(1), 121.90(3); P(1)−Cu−Cl(1), 95.27(3); P(2)−Cu−Cl(3), 93.34(3); P(1)−Cu−Cl(3), 123.22(3); Cl(1)−Cu−Cl(3), 89.55(3).

Group 4 and group 11 metal atoms have also been linked by all-carbon bridging ligands. Lang and co-workers reported the synthesis of alkynyl-titanocene derivatives $Cp_2Ti(C{\equiv}CR)_2$ (R = Ph, ^{t}Bu, $SiMe_3$, Fc,...) which behave as organometallic π-tweezers toward Cu(I).[14] We now wish to report a new use of a known titanocene-dichloride phosphane as metalloligand. This approach has the advantage of preserving intact the central $TiCl_2$ moiety of the titanocene, which subsequently provides additional possibilities for catalysis and electronic signaling via the metal-halide-metal bridge.[3d,15]

The metalloligand $CpTiCl_2Cp\text{-}PPh_2$ (**1**) is synthesized according to a reported procedure from the reaction of lithium(diphenylphosphino)cyclopentadienide with $CpTiCl_3$.[6] This phosphane is then treated with 0.5 equiv of $Cu(CH_3CN)_4PF_6$ to afford the novel cationic trimetallic complex **2**. Red crystals of compound **2** are obtained in 55% yield from slow diffusion of hexane into a CH_2Cl_2 solution of the compound. It crystallizes as a racemate in a centrosymmetric space group. Figure 1 shows the molecular structure of one of the enantiomers, and selected bond lengths and angles are reported below. The complex belongs to the C_2 point group (non crystallographic) with the central Cu atom coordinated to two titanocene dichloride phosphanes. One phosphorus and one chloride atom of each titanocene dichloride phosphane chelates the central Cu ion. The two titanocene moieties are oriented in orthogonal fashion, generating the expected tetrahedral geometry for a d^{10} Cu metal. The geometry about the Cu is best described as a flattened tetrahedron with the Cl−Cu−Cl and P−Cu−P angles equal to 89.55(3) Å and 128.81(4) Å, respectively.

Scheme 1

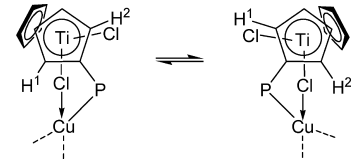

The Ti(1)−Cl(1) and Ti(2)−Cl(3) distances (both equal to 2.389(1) Å) are significantly longer than Ti(1)−Cl(2) and Ti(2)−Cl(4) (2.329(1) Å, 2.337(1) Å) which is consistent with bridging roles for the Cl(1) and Cl(3) atoms.

The $^{31}P\{^1H\}$ NMR spectrum of a single crystal of **2** exhibits a broad singlet at −3.1 ppm at room temperature which sharpens upon cooling and a septet at −144 ppm ($^1J_{PF}$ = 708 Hz) which is readily assigned to the anion PF_6^-. The broadening of the singlet at room temperature and the notably small downfield shift (Δ = 13.3 ppm) from the signal of the free phosphane **1** are consistent with coordination of the metalloligands to the labile d^{10} copper center.[16] The ^1H NMR spectrum of **2** exhibits only two multiplets for the α and β protons of the substituted cyclopentadienyl ring, one singlet for the unsubstituted Cp ring and one multiplet for the phenyl protons. Since no diastereotopic splitting of the substituted Cp in the ^1H and ^{13}C NMR (indicating the presence of the two chiral titanium centers) can be observed down to −70 °C, one might conclude that the titanocene-dichloride phosphane **1** is a hemilabile ligand and that the μ-Cl bridges are not persistent in solution. Nevertheless, considering the preference of copper(I) for a fully tetrahedral coordination, a fluxional process involving interchange of the coordinated and non-coordinated chlorides may also be at the origin of this phenomenon (Scheme 1).[4c] Unfortunately, the coalescence temperature in the VT-NMR experiments was not observed (−70 to 25 °C), so we could not speculate further.

The neutral trimetallic complex **3** is prepared from the reaction between phosphane **1** and CuCl in a 2:1 molar ratio. Suitable crystals of **3** for X-ray measurements were obtained by a layering technique (83% yield). The molecular structure of **3** is shown in Figure 2. In the solid state, the neutral Cu(I) complex exhibits primarily a trigonal planar coordination geometry built from two phosphanes and one chloride ligand. In addition, a weak interaction is also noted arising from a close contact of one chloride ligand bonded to one of the two titanium atoms, hence completing the coordination sphere of the copper atom. The Cu−Cl(1) bond length is 2.7571(6) Å which is consistent with a weak bonding interaction (Cu−Cl distances in **2** are about 2.42 Å). The slight deviation from 360° observed for the sum of the three angles around the trigonal copper (356.4°) also reveals the weakness of this interaction. Both titanocene fragments have a tetrahedral geometry and are aligned one behind the other.

The ^{31}P NMR spectrum of **3** exhibits a broad singlet at −11.9 ppm which corresponds to a downfield shift of only about 4.5 ppm relative to the free phosphane. The ^1H NMR spectrum exhibits just two ^1H resonances for the substituted Cp, one for the Cp and one for the phenyl groups. These

(13) (a) Nadasdi, T. T.; Stephan, D. W. *Organometallics* **1992**, *11*, 116. (b) White, G. S.; Stephan, D. W. *Inorg. Chem.* **1985**, *24*, 1499.
(14) Lang, H.; Stein, Th. *J. Organomet. Chem.* **2002**, *641*, 41.
(15) Leschke, M.; Lang, H.; Holze, R. *J. Solid State Electrochem.* **2003**, *7*, 518.
(16) Black, J. R.; Levason, W.; Spicer, M. D.; Webster, M. *J. Chem. Soc., Dalton Trans.* **1993**, 3129.

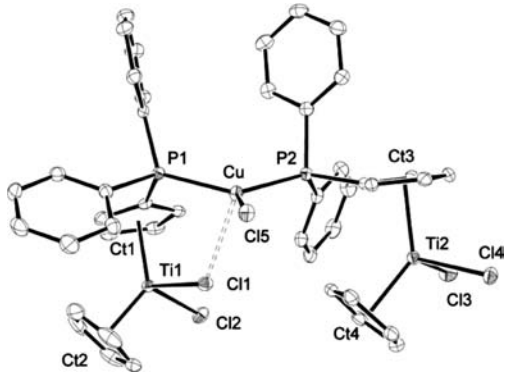

Figure 2. ORTEP representation of $[CpTiCl_2Cp\text{-}PPh_2]_2CuCl$ (**3**). The thermal ellipsoids are shown at 50% probability. The H-atoms and the three CH_2Cl_2 solvate molecules are not shown for clarity. Selected bond distances (Å) and angles (deg): Cu−P(1), 2.2692(6); Cu−P(2), 2.2721(6); Cu−Cl(5), 2.2765(6); Cu−Cl(1), 2.7571(6); Ti(1)−CT(1), 2.0671(5); Ti(1)−CT(2), 2.0507(6); Ti(1)−Cl(1), 2.3838(6); Ti(1)−Cl(2), 2.3405(7); Ti(2)−CT(3), 2.0851(5); Ti(2)−CT(4), 2.0461(5); Ti(2)−Cl(3), 2.3612(7); Ti(2)−Cl(4), 2.3585(6);P(1)−Cu−P(2),128.52(2);P(1)−Cu−Cl(5),114.04(2);P(2)−Cu−Cl(5), 113.86(2); P(1)−Cu−Cl(1), 81.538(19); P(2)−Cu−Cl(1), 109.70(2); Cl(1)−Cu−Cl(5), 97.413(19); CT(1)−Ti(1)−CT(2), 131.68(5); CT(3)−Ti(2)−CT(4), 133.16(4); Cl(1)−Ti(1)−Cl(2), 93.61(2); Cl(3)−Ti(2)−Cl(4), 94.98(2); Ti(1)−Cl(1)−Cu, 119.29(2).

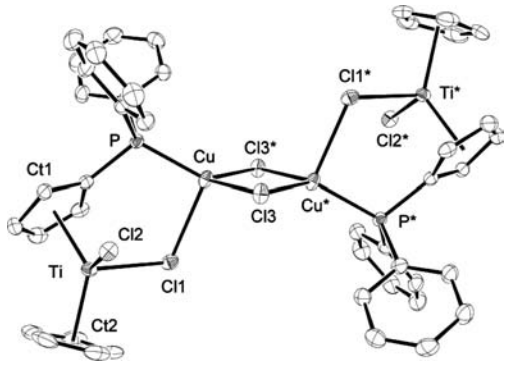

Figure 3. ORTEP representation of $[(CpTiCl_2Cp\text{-}PPh_2)Cu(\mu\text{-}Cl)]_2$ (**4**). The thermal ellipsoids are shown at 50% probability. The H-atoms and the CH_2Cl_2 solvate molecule are not shown for clarity. Selected bond distances (Å) and angles (deg): Ti−CT(1), 2.0809(6); Ti−CT(2), 2.0653(7); Ti−Cl(1), 2.3732(7); Ti−Cl(2), 2.3333(7); Cu−Cl(1), 2.5497(7); Cu−Cl(3), 2.3130(6); Cu−Cl(3)*, 2.3126(6); Cu−P, 2.1719(6); Cu···Cu*, 2.9724(6); Cu···Cl(2), 4.147(1); CT(1)−Ti−CT(2), 131.34(5); Cl(1)−Ti-Cl(2), 95.53(2); Ti−Cl(1)-Cu, 110.57(2);Cu−Cl(3)-Cu*, 79.97(2);P−Cu−Cl(3), 124.79(2);P−Cu−Cl(3)*, 124.19(2); Cl(3)−Cu−Cl(3)*, 100.03(2); P−Cu−Cl(1), 96.13(2); Cl(1)−Cu−Cl(3)*, 105.81(2); Cl(1)−Cu−Cl(3), 102.16(2).

data strongly suggest that the weakly coordinating chloride ligand observed in the solid state from one of the two titanium atoms does not persist in solution, so that both titanocene fragments become equivalent on the NMR time-scale.

Reaction between metalloligand **1** and CuCl in 1:1 ratio under similar conditions as for **3** yields the tetrametallic complex **4**. Thus, just by changing the reagent ratio, we can choose the nature of the product. Red crystals of compound **4** are obtained in 70% yield from slow diffusion of hexane into a CH_2Cl_2 solution of the compound. An Oak Ridge Thermal Ellipsoid Plot (ORTEP) representation of compound **4** is shown in Figure 3 along with selected bond distances and angles. In the solid state, the complex is crystallographically centrosymmetric with the center of symmetry located between the two copper atoms. Each organometallic phosphane chelates one copper atom. The two ligands are related

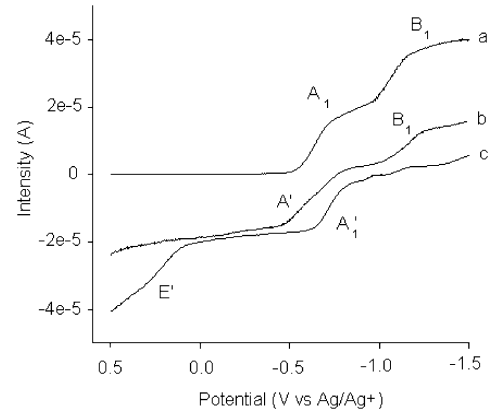

Figure 4. RDE voltammograms of **2** in a THF-$[N(nBu)_4][PF_6]$ solution. (a) **2** alone; (b) **2** after electrolysis at −0.8 V and consumption of one electron; (c) **2** after electrolysis at −1.1 V and consumption of a second electron.

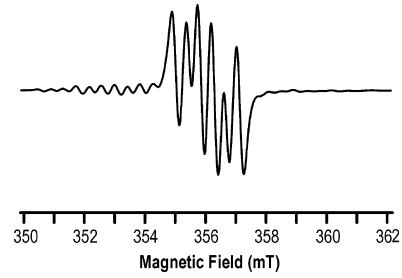

Figure 5. Isotropic solution EPR spectrum of $[(CpTiCl_2Cp\text{-}PPh_2)_2Cu]^0$ (**2′**) obtained from the 1-electron reduction of $[(CpTiCl_2Cp\text{-}PPh_2)_2Cu]^+$ (**2**).

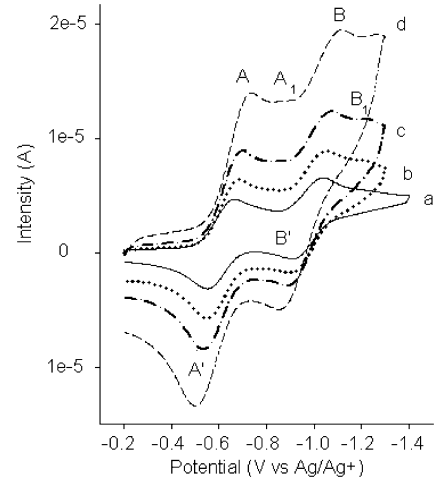

Figure 6. CVs of **2** in THF-$[N(nBu)_4][PF_6]$ solution. Starting potential: −0.2 V; Sweep rates: (a) 0.050; (b) 0.100; (c) 0.200; (d) 0.500 V s^{-1}.

by a center of inversion and are thus enantiomers. The geometry of the copper atoms is pseudo tetrahedral with structural parameters similar to those observed for other μ-chloro binuclear Cu(I) complexes $[L_2Cu(\mu\text{-}Cl)]_2$ reported in the literature.[17] Both titanium atoms exhibit a tetrahedral geometry and are oriented in opposite directions. The Cu−Cl(1) bond length (and its symmetric equivalent) is relatively short (2.5497(7) Å) which demonstrates further the ability of ligand **1** to adopt a bidentate (P, Cl) coordination mode in the solid state. The NMR analysis of **4** is analogous to **2** and **3**, displaying a broad singlet at −5.9 ppm

(17) Bayler, A.; Schier, A.; Schmidbaur, H. *Inorg. Chem.* **1998**, *37*, 4353.

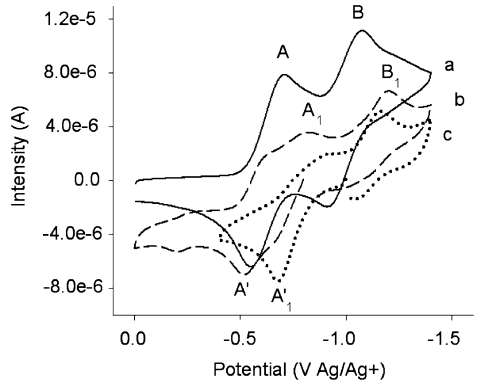

Figure 7. CVs of **2** in THF-$[N(nBu)_4][PF_6]$ solution. (a) **2** alone starting potential 0 V, sweeprate 0.050 $V.s^{-1}$; (b) after electrolysis at −0.8 V and consumption of one electron. Starting potential −0.8 V; (c) after electrolysis at −1.1 V and consumption of a second electron. Starting potential −1 V.

in the ^{31}P NMR spectrum and the ^{1}H and ^{13}C signals associated with the titanocene moiety are without any diastereotopic splitting of the substituted Cp. These data suggest again the hemilability of the titanocene-dichloride phosphane ligand in solution.

Electrochemistry. The cationic complex $[(CpTiCl_2Cp\text{-}PPh_2)_2Cu]^+$ (**2**) in tetrahydrofuran (THF, 0.2 M $TBAPF_6$) exhibits two well-defined reduction waves A_1 and B_1 at −0.67 and −1.07 V versus Ag/Ag^+ in the steady state RDE voltammograms. The current amplitudes of these waves are nearly of equal intensity and correspond to a 1-electron process (Figure 4; trace a).

We assign these processes to the successive reduction of Ti(IV) → Ti(III) (eqs 1 and 2). This assignment is supported by EPR findings (Figure 5) and DFT computations (below).

$$\text{Ti}'(\text{IV})\text{-Cu(I)-Ti(IV)} + 1e^- \overset{A_1}{\rightleftharpoons} \text{Ti}'(\text{III})\text{-Cu(I)-Ti(IV)} \qquad -0.67\ \text{V} \quad (1)$$

$$\text{Ti}'(\text{III})\text{-Cu(I)-Ti(IV)} + 1e^- \overset{B_1}{\rightleftharpoons} \text{Ti}'(\text{III})\text{-Cu(I)-Ti(III)} \qquad -1.07\ \text{V} \quad (2)$$

In the cyclic voltammograms (CVs) using a sweep rate of 200 mV/s (Figure 6), two well-defined reversible systems are depicted A/A′ and B/B′. However, at faster scan rates, shoulders A_1 and B_1 are depicted for which their intensities increase with the sweep rate. Since waves A and B are placed at lower negative potentials with respect to that of A_1 and B_1, respectively, this means that the former species are more easily reduced.

These observations (RDE vs CV; sweep rate dependence) indicate that a C/E process (C = chemical; E = electrochemical) takes place. The explanations are as follows. The presence of two peaks and the observed decrease in electronic density at the Ti center (since the reduction potentials are not the same) are explained by a Cl-atom transfer from the Ti to the Cu induced by the electrochemical process as shown in the Scheme 2.

Scheme 2

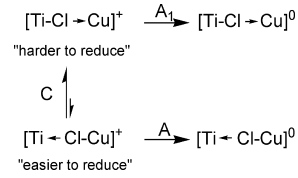

Scheme 3

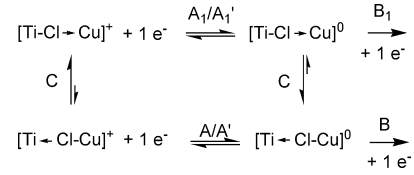

The bulk electrolysis applied at −0.8 V versus Ag/Ag^+ (at wave A_1), leads to a species exhibiting oxidation waves A′ and A_1', and a reduction wave B_1 after consuming nearly 1 F (Figure 4, trace b). The CV of this reduced species exhibits oxidation peaks A_1' and A′ and reduction peaks A, A_1, and B_1 (and a weaker shoulder B) during a cathodic scan (Figure 7, trace b). The overall results can be summarized as a square scheme derived from Scheme 2 (Scheme 3). Because four peaks altogether are observed in the CV, the electrolytic solution contains many species in equilibrium. The reduced species formulated as $[Ti-Cl\rightarrow Cu]^0$ and $[Ti\leftarrow Cl-Cu]^0$ exhibit reduction waves B_1 and B, and oxidation waves A_1' and A′, respectively. The presence of the paramagnetic species, $[Ti\leftarrow Cl-Cu]^0$, is confirmed by EPR (Figure 5). The absence of the species $[Ti-Cl\rightarrow Cu]^0$ is due to its relative instability evolving toward the former with the EPR time scale of the experiment. Moreover in the CV, all waves appear as reversible; it is reasonable to assume that Cl anion elimination does not occur.

When the bulk electrolysis is further carried out at −1.1 V versus Ag/Ag+ (at wave B_1), the RDE voltammogram exhibits two oxidation waves A_1' and E′ at (+0.25 V) after nearly 1 consumed electron (Figure 4; trace c). The CV of the resulting solution exhibits only the oxidation wave A_1' and the reduction waves A_1 and B_1 (Figure 7; trace c). Because the wave potentials are quasi-identical and the shape of the peaks observed in the CV are very similar to that described above, this second 1-electron reduction process must occur at the second Ti center.

The anionic species is unstable as peak B_1 is irreversible meaning that a Cl^- anion must be eliminated during this process. This conclusion is supported by the appearance of the typical oxidation wave (E′) associated to the presence of uncoordinated Cl^- anions (Figure 4; trace c). The resulting solution exhibits an identical EPR spectrum to the former one (Figure 5) clearly indicating the formation of a species best formulated as Ti′(III)−Cu(I)−Ti(III). On the basis of the fact that the only oxidation wave observed belongs to both Ti centers at the same time (wave A_1'), one can reasonably assume that the chemical environment about both Ti metals is the same, that is, a symmetric complex (Chart 1).

Under the same experimental conditions as indicated above, compound **3**exhibits by RDE voltammetry two

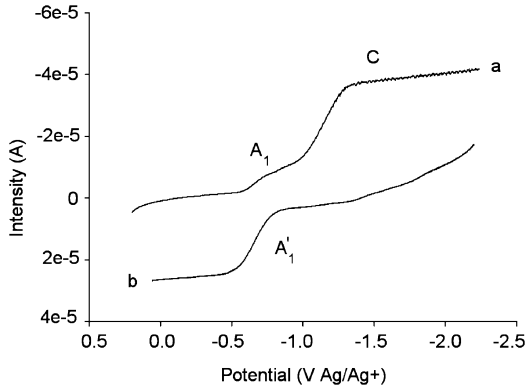

Figure 8. RDE voltamograms of **3** in THF-$[N(nBu)_4][PF_6]$ solution. (a) **3** alone; (b) **3** after electrolysis at −1.2 V and consumption of two electrons.

Chart 1

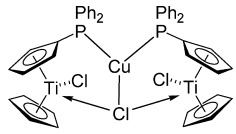

5

reduction waves A and C. The height of wave A is smaller than that for C. The presence of wave A suggests that an oxidation of compound **3** occurs under the influence of an electrochemical reaction (chemical/electrochemical process; CE mechanism) (Figure 8). After the electrolysis performed at −1.3 V (plateau of wave C) and the consumption of two electrons (*n* experimental = 1.95 F), the RDE voltammogram of the resulting solution exhibits a well defined oxidation wave A'_1. An intense peak is observed in the EPR spectrum which is identical to that previously mentioned above, in agreement with the quantitative formation of **5**.

The CV measurements for **4** as performed using a rotating disk electrode in THF and in the presence of 0.2 mol $L^{-1}[N(nBu)_4][PF_6]$ as the supporting electrolyte exhibit two well-defined reduction waves D and E at −0.75 and −1.10 V, respectively. In the CV, two quasi- reversible systems D/D'_1(ΔEp = 250 mV) and E/E'_1 (ΔEp = 270 mV) are detected (Figure 9). When an electrolysis is performed at −0.85 V (plateau of wave D), 1 F is consumed and the oxidation wave D'_1 is observed. By EPR spectroscopy, a well defined resonance appears, which is very similar to that observed previously (Figure 5). After a second electrolysis (performed at −1.2 V at the plateau of wave E), another electron is consumed, and the RDE voltammogram of the resulting solution exhibits the same oxidation wave D'_1. By EPR spectroscopy, the same spectrum as described above is obtained (Figure 5).

As the same oxidation peak D'_1 and the same EPR spectrum were obtained after one or two consumed electrons, we can postulate the following mechanism (Scheme 4).

All in all, whatever the starting compound **2**, **3**, and **4** is, the 1- or 2-electron reduction processes lead to a product that is oxidizable in the same potential range (peak A'_1). It is particularly striking that the EPR spectra are essentially identical for all cases including the various coupling constants. This result shows that the electron is relocated in the same way on the fragments containing Ti, P, Cu, and Cl.

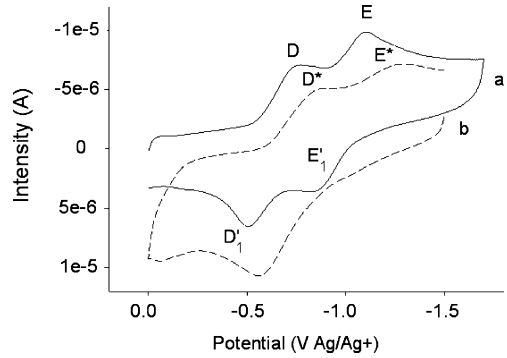

Figure 9. CVs of **4** in THF-$[N(nBu)_4][PF_6]$ solution. (a) **4** alone starting potential 0V; (b) **4** after one electron at −0.85V.

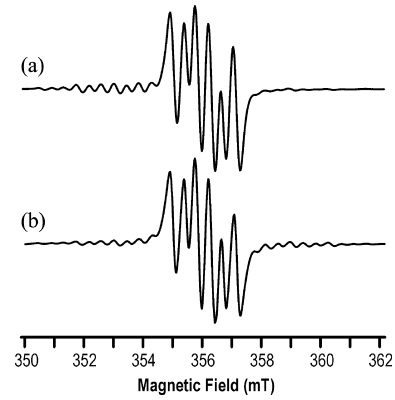

Figure 10. Experimental (a) isotropic solution EPR spectrum of $[(CpTiCl_2Cp\text{-}PPh_2)_2Cu]^0$ (**2′**) obtained from the 1-electron reduction of $[(CpTiCl_2Cp\text{-}PPh_2)_2Cu]^+$ (**2**) and simulation (b) performed with Bruker SimFonia ver. 1.25. The simulation employed the following parameters: $a(^{31}P)$ = 8.00, $a(^{63/65}Cu)$ = 4.43/4.47, $a(^{47/49}Ti)$ = 12.77 Gauss; 100% Lorentzian line shape and a line width of 2.30 G.

Scheme 4

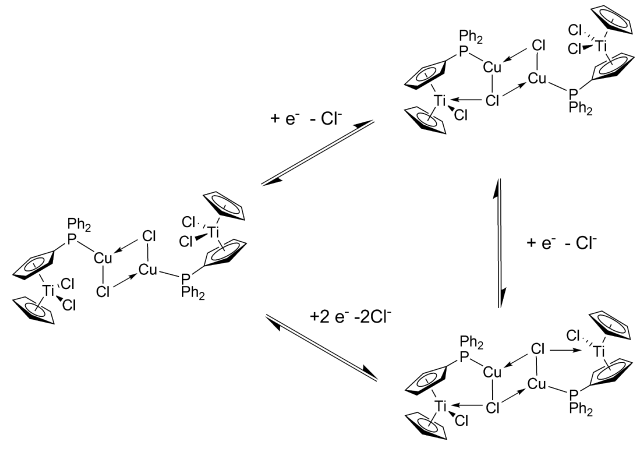

EPR Analysis of Neutral $[(CpTiCl_2Cp\text{-}PPh_2)_2Cu]^0$. The spectrum of $[(CpTiCl_2Cp\text{-}PPh_2)_2Cu]^0$ (**2′**) was obtained from the cationic trinuclear complex **2**. However, simulation of the EPR spectrum represents a very good fit for hfc to *one* ^{31}P, *one* $^{63/65}Cu$, and *one* $^{47/49}Ti$ nucleus, with coupling constants of 8.00, 4.43/4.47, and 12.77 Gauss, respectively (Figure 10). The spectrum displays fully Lorentzian lines with a fitted line width of 2.3 Gauss, and has a *g* value of 1.978. Thus, there seems to be little evidence for the presence

of unresolved hfc (which tends to lead to Gaussian lineshapes), and both the linewidths and g values are comparable to those observed for other Cp_2Ti-based paramagnetic complexes. Thus, for example, the EPR spectra recorded for $[Cp_2TiCl]$ in THF has $g = 1.976$, $a(^{47/49}Ti) = 14.6$ Gauss, and a line width of 2.0 Gauss.[18] The mixed Ti/Cu paramagnetic complex $[(Cp_2TiSCH_2CH_2CH_2S)_2Cu]$ has $g = 1.9821$, $a(^{47/49}Ti) = 10.5$ Gauss and $a(^{63}Cu) = 3.5$ Gauss.[13a]

DFT calculations (below) indicate that upon reduction of **2**, a symmetry-reduction of the frontier orbitals occurs (equivalent to a classical description of a Ti(III)/Cu(I)/Ti(IV) mixed-valence state). Such a process, which induces localization of the unpaired electron density onto *one* Ti, easily explains the observed coupling to a single Ti nucleus, but it is more difficult to understand how coupling occurs to only a single ^{31}P nucleus, given both the large nuclear g-value of phosphorus and the apparent presence of considerable spin density on the copper atom. Thus, it must be considered that the observed symmetry reduction leads to partial dissociation of ligands from the Cu(I) center. This conclusion is supported by DFT (below) but also corroborates the electrochemical behavior of this complex as described above.

Finally, we note that an almost equally good EPR simulation could be obtained for coupling to a single Cl atom in place of the Cu, for which the calculated $a(^{35/37}Cl)$ values are 4.63 and 3.85 Gauss, respectively. This is because both these elements have a major isotope with $I = 3/2$ of similar natural abundance (69.17 vs. 75.78%). Against the notion that reduction has decomplexed the copper to yield, for example, a paramagnetic $[CpTiCp'Cl]$ is the fact that the EPR spectrum of $[Cp_2TiCl]$ does not exhibit any hfc to chlorine at all.[18] However, the presence of the PPh_2 side-group on the Cp ring in Cp′ might alter this situation and lead to an interaction that induces spin density onto the Cl nucleus.

Computations and Frontier MOs. To calibrate our computational methodology, the geometry of the diamagnetic cationic species $[(CpTiCl_2Cp\text{-}PPh_2)_2Cu]^+$ (**2**) (see Supporting Information, Figure S1) was optimized by DFT (the comparison of selected bond distances and angles is placed in the Supporting Information, Figure S2). Although the basic skeleton was fairly well reproduced as well as the symmetry of the ClTi−Cl−CuP_2−Cl−TiCl core (i.e., point group C_2) by DFT computations, some distances exhibit discrepancies, notably those about the Cu(I) metal (Cu−P and Cu−Cl) and the bridging Cl-atoms. Consequently, this DFT analysis can only be used in a comparative sense between the computed cation structure of $[(CpTiCl_2Cp\text{-}PPh_2)_2Cu]^+$ (**2**) and the computed neutral species $[(CpTiCl_2Cp\text{-}PPh_2)_2Cu]^0$ (**2′**). The optimized geometry for $[(CpTiCl_2Cp\text{-}PPh_2)_2Cu]^0$ (**2′**) (Supporting Information, Figure S3) exhibits a similar ClTi−Cl−CuP_2−Cl−TiCl core structure as in (**2**) except that significant variation in some distances, primarily involving bonds to bridging chlorine atoms, occur (Figure 11), rendering the reduced species distinctly unsymmetrical.

The computed terminal Ti−Cl distances are 2.37 and 2.48 Å indicating weaker interactions on one side. These weaker

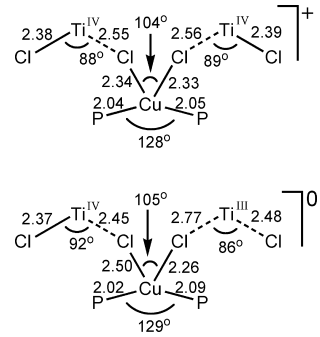

Figure 11. Comparison of selected bond distances (Å) and angles of the skeleton found in the optimized geometry of $[(CpTiCl_2Cp\text{-}PPh_2)_2Cu]^+$ (up: **2**) and $[(CpTiCl_2Cp\text{-}PPh_2)_2Cu]^0$ (down: **2′**) using DFT (B3LYP with basis sets 3-21G* for Ti, Cl, Cu, P, and C′s of Cp′s, and molecular mechanics UFF with basis sets STO-3G for C′s of Ph and H′s).

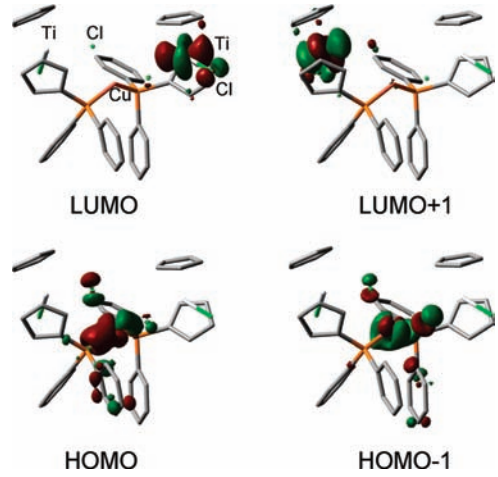

Figure 12. Drawings of the four frontier MOs of the diamagnetic $[(CpTiCl_2Cp\text{-}PPh_2)_2Cu]^+$ complex (**2**).

interactions indicate a gain in electron density rendering one of the Ti atoms less cationic and so inducing weaker electrostatic interactions. This conclusion also suggests a possible enhanced lability of the reduced metallo-ligand. The calculated terminal Ti−Cl distances on the other side do not change very much upon reduction, suggesting that the gain in electron density occurs primarily at a single Ti center. That the computed Cu−P distances undergo relatively minor perturbation confirms that reduction does not occur at copper.

This localized reduction is also confirmed from an analysis of the frontier MOs. Two pairs of frontier orbitals are quasi-degenerate (LUMO+1, −0.200; LUMO, −0.208; HOMO, −0.291; HOMO-1, −0.296 au; Figure 12) because of a small difference in phenyl group orientations in the computed static structure. More importantly, the atomic contributions to these MOs are essentially identical, which is entirely consistent with the X-ray structure data. On the other hand, the HOMO and HOMO-1 do not exhibit similar atomic distributions, so that their similarity in energy is probably accidental. In both latter cases, the MOs are mainly located in the Cu(I) metal meaning that any oxidation process would remove an electron from this metal center. This observation is consistent with the d^{10} electron-rich configuration of the metal. Conversely, the d^0 electronic configuration of Ti(IV) suggests that reduction should take place there.

(18) Samuel, E.; Vedel, J. *Organometallics* **1989**, *8*, 237.

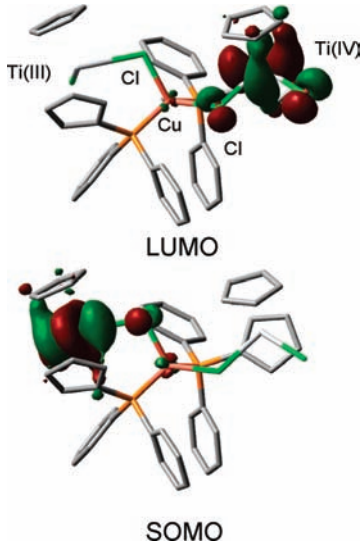

Figure 13. Drawings of the four frontier MOs of the diamagnetic $[(CpTiCl_2Cp\text{-}PPh_2)_2Cu]^0$ complex (**2′**).

Since the computed structure of **2′** is geometrically unsymmetrical, orbital degeneracy is not expected; this is indeed observed with the, SOMO (−0.161) and LUMO (−0.087 au) well separated in energy (Figure 13). Although one may intuitively assume that the next one-electron reduction should take place in the SOMO based on an examination of this simplified MO diagram, in reality as experimentally demonstrated by electrochemical experiments, the next reduction takes place at the Ti(IV) center. This apparent discrepancy is resolved by considering the CE mechanism determined from the electrochemical experiments. We thus postulate that the minor species $[Ti{\leftarrow}Cl{-}Cu]^+$, is the most easily reducible and yet is consumed first. So, a CE mechanism explains this discrepancy. This alters the electronic structure of the monocation and a second reduction step at the remaining Ti(IV) center subsequently occurs, but at higher potential. It cannot be expected that a gas-phase calculation can accurately mimic this follow-up reaction, given that the influence of solvent and electrolyte are not included. Furthermore, given the large number of possible geometries and conformations that the actual reduced product might adopt, we consider it quite unrealistic to computationally probe this system further.

Conclusion

We have described the synthesis of two new heterotrinuclear complexes **2** and **3** containing two Ti(IV) d^0 ions and one Cu(I) d^{10} ion. These syntheses involve the reaction of the metalloligand $CpTiCl_2Cp\text{-}PPh_2$ with either $Cu(MeCN)_4PF_6$ or CuCl in a 2:1 ratio. Variation of the ratio of the ligand versus CuCl led to the synthesis of a tetranuclear Ti−Cu−Cu−Ti complex **4**. X-ray diffraction studies show strong bonding interactions between the chloride atoms of the metalloligand and the Cu(I) center in the complexes **2** and **4** although NMR studies suggest potential hemilability of the early metal ligand in solution.

The electrochemical findings, as well as the EPR and DFT analyses, indicate remarkably weak electronic communication between the two Ti centers in the reduced forms of these heteropolynuclear complexes. Despite this, two fully chemically reversible reduction steps are observed leading to products with distinct Ti(III) character. The remarkable versatility of this system appears to be enabled by an efficient chloride ion shuttle between the Ti and Cu centers. This observation contrasts strongly with the *trans*-$PtL_2(C{\equiv}CFc)_2$ and $Pt_2(dppm)_2(C{\equiv}CFc)_2$ complexes where Fc = ferrocenyl, L = phosphine, dppm = bis(diphenylphosphino)methane.[19,20] While in these latter cases the CVs also exhibit two sequential one-electron steps (albeit oxidations), there it is caused by strong electronic coupling between the (conjugated) Fc centers. Thus, what on casual analysis may appear to be very similar electrochemical responses in two ligand-bridged trimetallic systems, upon a more thorough analysis are shown to be fundamentally different mechanisms.

Acknowledgment. The Natural Sciences and Engineering Research Council of Canada (NSERC) and the Centre National de Recherche Scientifique (CNRS, UMR 5260) are acknowledged for funding. P.D.H. thanks CEMOPUS (Centres d′Études des Matériaux Optiques et Photoniques de l′Université de Sherbrooke) for fundings.

Supporting Information Available: Optimized geometry of $[(CpTiCl_2Cp\text{-}PPh_2)_2Cu]^+$ (**2**) and $[(CpTiCl_2Cp\text{-}PPh_2)_2Cu]^0$ (**2′**), and comparison of selected structural data between the X-ray and DFT results for $[(CpTiCl_2Cp\text{-}PPh_2)_2Cu]^+$ (**2**). This material is available free of charge via the Internet at http://pubs.acs.org.

IC8023869

(19) Yip, J. H. K.; Wu, J.; Wong, K.-Y.; Ho, K. P.; Pun, C. S.-N.; Vittal, J. J. *Organometallics* **2002**, *21*, 5292.
(20) Osella, D.; Gobetto, R.; Nervi, C.; Ravera, M.; D′Amato, R.; Russo, M. V. *Inorg. Chem. Commun.* **1998**, *1*, 239.